Risk Quantification for Automated Driving using Information from V2V Basic Safety Messages

Raghvendra V. Cowlagi* Rebecca C. Debski* Alexander M. Wyglinski†
*Aerospace Engineering Department †Electrical & Computer Engineering Department
Worcester Polytechnic Institute, 100 Institute Rd., Worcester, MA, USA 01609.

***Abstract*—Using data from V2V links along with onboard sensor data is recognized as a crucial step towards the safety and reliability of future automated driving. We address short-term trajectory planning for the ego vehicle. We propose a threat field model of the traffic surrounding the ego vehicle. Informally, the threat field indicates the possibility of collisions in the vehicle's vicinity. We study uncertainty in the threat field due to uncertainty in the positions and velocities of surrounding vehicles, which may be known to the ego CAV via basic safety messages. The cost of trajectories is defined by the expected threat exposure, and the risk of trajectories is quantified based on the variance in cost. Uncertainty quantification is studied using Monte Carlo sampling as well a perturbation-based approach. The main result of this paper is the observation that small localization errors and/or speed measurement errors can lead to large risks in planned trajectories.**

***Index Terms*—Connected automated vehicles, risk, vehicle-to-vehicle communications, trajectory planning.**

I. Introduction

Connected automated vehicles (CAVs) obtain information about the local environment and traffic from multiple sources including onboard sensors and data received from vehicle-to-vehicle (V2V) communications [1]. All current automated vehicles (AVs), regardless of the level of autonomy, carry multiple onboard sensors including optical cameras, radar, and lidar. Various manufacturers use proprietary methods for extracting and fusing information from onboard sensor data.

Using data from V2V links along with onboard sensor data is recognized as a crucial step towards the safety and reliability of future automated driving [2]. The literature on using V2V data for automated driving mainly addresses cooperative scenarios such as platooning, cf. [3]–[6]. However, the current trend of advances in automated driving points to scenarios of *independent* driving, where each vehicle plans and executes its own actions without expecting cooperation from other vehicles. In what follows, we refer to an *ego* CAV for which we are interested in enabling automated driving.

In noncooperative scenarios, it is important to quantify the *risk* associated with actions planned by the ego CAV. This risk arises from uncertainty in the knowledge (e.g., positions, velocities, and accelerations) of surrounding traffic.

We address the specific automated driving task of short-term trajectory planning for the ego CAV. Such trajectories are continually planned by AVs to serve higher-level planning objectives such as lane-keeping, lane-changing, and waypoint navigation. Trajectory planning under uncertainty is generally addressed as an optimization or optimal control problem to minimize an expected cost function [7], [8]. The surrounding environment is typically represented by probabilistic occupancy maps (POMs) [9]–[11]. In this paper we address the problem of trajectory *risk* quantification for the ego CAV using data from basic safety messages (BSMs) via V2V communications. BSMs may include the current position, velocity, and/or acceleration of surrounding vehicles.

We propose a threat field model of the traffic surrounding the ego CAV, where a spatiotemporally varying scalar field is constructed. Informally, the threat field indicates the possibility of collisions in the surrounding environment, similar to POMs. Desirable trajectories are characterized as those with low or minimum threat exposure. We study uncertainty in the threat field due to uncertainty in the positions and velocities of surrounding vehicles, which may be known to the ego CAV via BSMs. The cost of trajectories is defined by the expected threat exposure, and the risk of trajectories is quantified by the variance in cost. Uncertainty quantification is studied using Monte Carlo sampling as well a perturbation-based approach.

The contributions of this paper are as follows. First, we propose a new threat field model for short-term trajectory planning in automated driving. This threat field model provides a framework to fuse V2V data with onboard sensor data, which is mathematically more convenient compared to the probabilistic occupancy grids typically used. The details of such data fusion are beyond the scope of this paper. Second, we analyze the effects of uncertainty in the positions and velocities of surrounding vehicles on the threat field. We provide methods to calculate the statistical characteristics (moments) of the threat field. Finally, we quantify risk of planned trajectories based on threat field uncertainty.

The rest of this paper is organized as follows. We introduce the threat field model in Section II, study its statistical characteristics in Section III, quantify trajectory risk in Section III-C, and conclude the paper in Section IV. In what follows, we denote by $\mathbb{R}$ the set of reals, by $\mathbb{R}^{n\times m}$ the set of matrices of size $n \times m$, by $I_{(n)} \in \mathbb{R}^{n\times n}$ the identity matrix, and by $\mathbb{E}[\cdot]$ and $Var[\cdot]$ the expected value and variance.

II. Threat Field Definition

In this section we define a spatiotemporally varying *threat field* c that models the possibility of collisions perceived by the ego CAV. Such a threat field is not unique. For example,

Funding acknowledgement: US National Science Foundation #1646367.

an aggressive driver may perceive the threat of collisions differently compared to a defensive driver. The following definition is based on safety recommendations by the US National Highway Traffic Safety Administration (NHTSA).

Consider a ego-fixed Cartesian axes system attached to the ego CAV such that the origin is at the vehicle's center of mass, the x-axis is tangential to the vehicle's lane on the road, the z-axis is perpendicular to the road and the y-axis completes a right-handed triplet. For the purposes of short-term trajectory planning, a section of the road $\mathcal{W}$ surrounding the ego CAV is considered. For simplicity, we assume $\mathcal{W}$ is a rectangular region that extends up to 200 m (typical onboard radar sensor range) in each direction along the x-axis and spans the entire width of the road along the y-axis.

We denote by $\boldsymbol{p} = (x, y)$ the spatial variable with coordinates in this axes system, by t the time, and by $\boldsymbol{p}_i(t) = (p_{ix}(t), p_{iy}(t))$ the coordinates of the relative position and relative velocity of other surrounding vehicles, respectively, for $i = 1, 2, \ldots, N$. Here N is the number of other vehicles.

We assume a nominal speed v_0 associated with the ego CAV's traffic situation. For example, in free-flow traffic on a highway, v_0 may be set equal to the regulatory speed limit. The NHTSA recommends a safe following distance (i.e., separation) per the "three-second rule," which is a speed-dependent separation. We denote by d_{ix} the desired separation to the i^{th} vehicle and encode the "three-second rule" as $d_{ix} := 3\,(v_0 + |v_{ix}|)$. Similarly, we denote by d_{iy} the desired lateral separation, which can be set to a constant based on lane width. We set $d_{iy} := 2$ m for each $i = 1, 2, \ldots, N$.

We define the threat field on $\mathcal{W}$ as a summation of collision threats to each of the N surrounding vehicles. The collision threat to the i^{th} other vehicle is modeled by a 2D lognormal function such that the peak of the function occurs at the relative position $\boldsymbol{p}_i$ of the other vehicle and the function value remains above a prespecified threshold $\varepsilon_0 \ll 1$ within a safe separation distance, as illustrated in Fig. 1. The asymmetry in the lognormal function depends on the relative velocity $\boldsymbol{v}_i$, e.g., a positive v_{ix} is associated with a "forward" skew.

We consider a lognormal function of the general form $f(x) = \exp(-\frac{1}{2}(\frac{\ln x - \beta}{\alpha})^2)$, where α and β are parameters to be chosen. We obtain the desired peak location and separation as illustrated in Fig. 1 for the i^{th} vehicle by choosing

$$
\begin{aligned}
\alpha_{ix}(t) &:= \varepsilon_1 \ln\left(\frac{v_0 + |v_{ix}(t)| + \varepsilon_2}{v_0 - |v_{ix}(t)| - \varepsilon_2}\right),\\
\alpha_{iy}(t) &:= \varepsilon_1 \ln\left(\frac{\varepsilon_3 + |v_{iy}(t)| + \varepsilon_4}{\varepsilon_3 - |v_{iy}(t)| - \varepsilon_4}\right),\\
\beta_{ix}(t) &:= \ln\left(d_{ix}\frac{v_0 - |v_{ix}(t)| - \varepsilon_2}{2(|v_{ix}(t) + \varepsilon_2|)}\right),\\
\beta_{iy}(t) &:= \ln\left(d_{iy}\frac{\varepsilon_3 - |v_{iy}(t)| - \varepsilon_4}{2(|v_{iy}(t) + \varepsilon_4|)}\right),
\end{aligned}
$$

where $\varepsilon_1 := 1/\sqrt{-\ln(\varepsilon_0^2)}$ and $\varepsilon_2, \varepsilon_4 \ll 1$ and $\varepsilon_3 \ll v_0$ are user-specified positive constants. To align the peak of the lognormal function with the vehicle's position, we define

$$
\begin{aligned}
\delta_{ix}(\boldsymbol{p}, t) &:= (\operatorname{sgn} v_{ix}(t))(x - p_{ix}(t)) + \exp(\beta_{ix}(t)),\\
\delta_{iy}(\boldsymbol{p}, t) &:= (\operatorname{sgn} v_{iy}(t))(y - p_{iy}(t)) + \exp(\beta_{iy}(t)).
\end{aligned}
$$

The collision threat for the i^{th} vehicle is then defined as:

$$
c_i(\boldsymbol{p}, t) := \exp\left(\frac{-(\ln(\delta_{ix}) - \beta_{ix})^2}{2\alpha_{ix}^2}\right)\exp\left(\frac{-(\ln(\delta_{iy}) - \beta_{iy})^2}{2\alpha_{iy}^2}\right)
$$

whenever $\delta_{ix}(\boldsymbol{p}, t) > 0$ and $\delta_{ix}(\boldsymbol{p}, t) > 0$. Otherwise, $c_i(\boldsymbol{p}, t) := \varepsilon_5$ otherwise, where $\varepsilon_5 \ll 1$ is a user-specified positive constant. Finally, the threat field is defined as the summation of collision threats for each of the N other vehicles:

$$
c(\boldsymbol{p}, t) := \varepsilon_6 \textstyle\sum_{i=1}^{N} c_i(\boldsymbol{p}, t). \tag{1}
$$

In this paper, we choose the following values of the various constants identified above.

$$
\begin{aligned}
&v_0 = 24.20 \text{ m/s } (55 \text{ mph}), \quad \varepsilon_0 = 0.1, \quad \varepsilon_2 = 0.2420,\\
&\varepsilon_3 = 5, \quad \varepsilon_4 = 0.05, \quad \varepsilon_5 = 1\text{E-}4 \quad \varepsilon_6 = 100.
\end{aligned}
$$

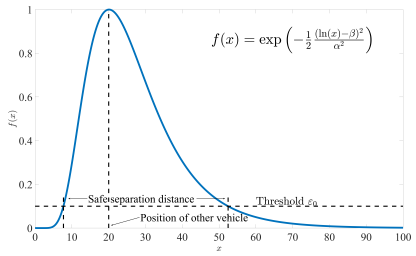

Fig. 1. Illustration of a 1D lognormal function with parameters α and β.

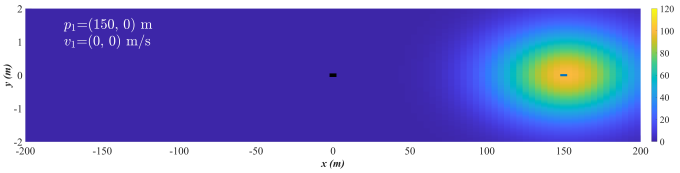

(a) $\boldsymbol{p}_1(t) = (150, 0)$ m and $\boldsymbol{v}_1(t) = (0, 0)$ m/s.

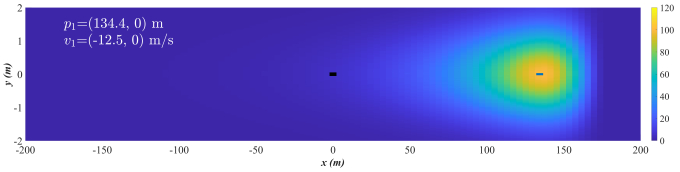

(b) $\boldsymbol{p}_1(t) = (134.4, 0)$ m and $\boldsymbol{v}_1(t) = (-12.5, 0)$ m/s.

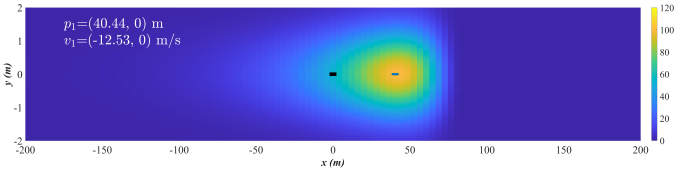

(c) $\boldsymbol{p}_1(t) = (40.44, 0)$ m and $\boldsymbol{v}_1(t) = (-12.53, 0)$ m/s.

Fig. 2. An illustration of the threat field with $N = 1$.

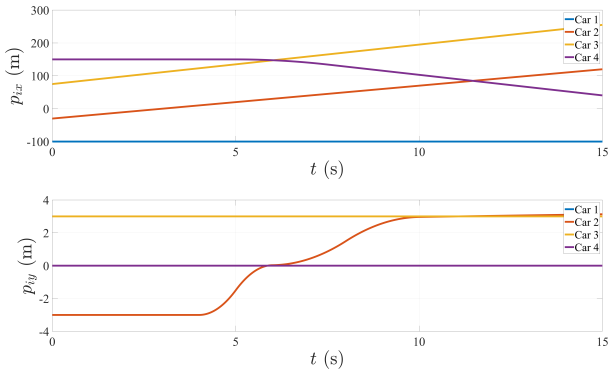

(a) Relative positions.

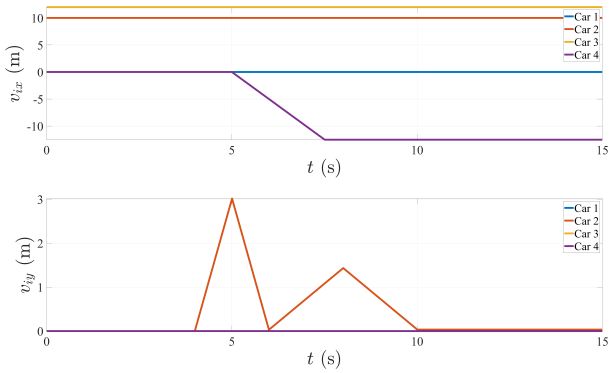

(b) Relative velocities.

Fig. 3. Positions and velocities in 4-car traffic scenario.

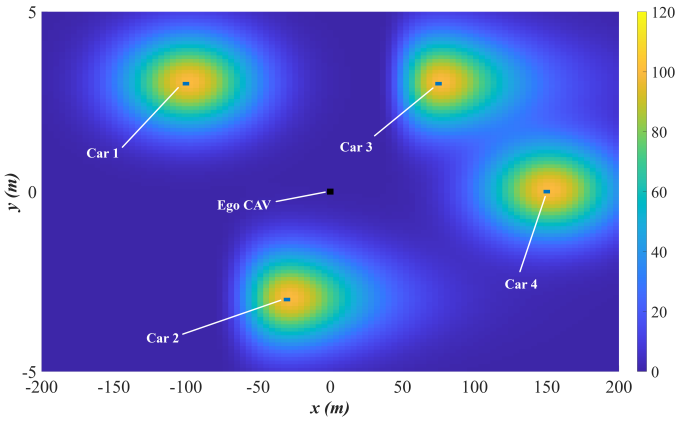

(a) $t = 0$ s.

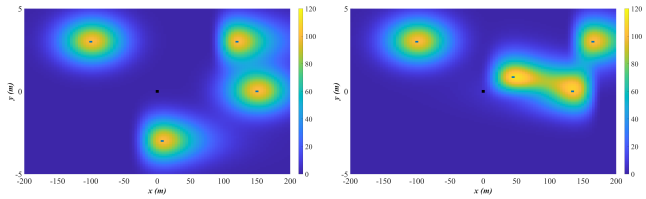

(b) $t = 3.75$ s.

(c) $t = 7.5$ s.

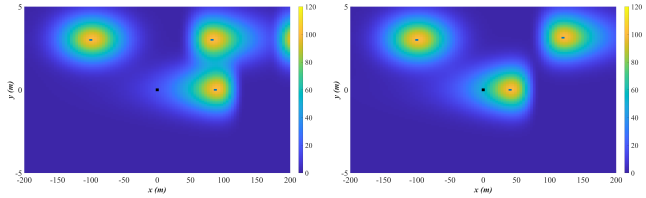

(d) $t = 11.25$ s.

(e) $t = 15$ s.

Fig. 4. Illustration of $c(\boldsymbol{p}, t)$ at various time instants in 4-car traffic scenario.

In this threat field, the positions and velocities of surrounding vehicles, $\boldsymbol{p}_i$ and $\boldsymbol{v}_i$, may be considered time-varying parameters. Figure 2 illustrates examples of $c(\boldsymbol{p}, t)$ with $N = 1$ at a particular time instant t for various values of $\boldsymbol{v}_1(t)$ and $\boldsymbol{p}_1(t)$.

Another illustrative example consists of $N = 4$ other cars on a three-lane road. Consider a traffic scenario where the positions and velocities of other cars relative to the ego CAV change over a 15 s time interval as shown in Fig. 3. Informally, Car 2 quickly moves from the right lane (lowermost in Fig. 4(a)) to the left lane and in the process moves in between the ego CAV and Car 4. While the ego CAV's line of sight to Car 4 is blocked by Car 2, Car 4 decelerates by a large amount. This traffic scenario, which is modeled after a real-world traffic accident [12], may be used in the future as a benchmark to demonstrate the benefits of connectivity, because onboard line-of-sight sensors will not suffice for the ego CAV to avoid collision with Car 4. Figure 4 shows the threat field at various time instants in this traffic scenario.

III. Threat Uncertainty Quantification

The relative positions and velocities $\boldsymbol{p}_i$ and $\boldsymbol{v}_i$ of surrounding vehicles may be known to the ego CAV via BSMs transmitted by the surrounding vehicles. The underlying assumption is that each vehicle can localize its poistion and estimate its velocity, e.g., using the Global Positioning System (GPS). Typical user error characteristics of position and velocity estimates using GPS are well-known. As of May 2016, 95% of the user range errors (URE) in horizontal position measured by GPS were less than 0.715 m and 95% of the user range rate errors (URRE) were less than 6E-3 m/s [13].

The main result of this paper is the observation that these "small" localization errors and/or speed measurement errors can lead to large uncertainties in the threat perceived by the ego CAV, which may consequently lead to a large risk in planned trajectories.

A. Monte Carlo Sampling

To address the problem of quantifying uncertainty in the threat $c(\boldsymbol{p}, t)$ dependent on the uncertain parameters $\boldsymbol{p}_i(t)$ and $\boldsymbol{v}_i(t)$, $i = 1, \ldots, N$, we consider the approach of Monte Carlo sampling [14]. Here, we first recognize that each parameter is a random variable that we assume to be normally distributed with mean values as transmitted in the BSMs and variances provided by the aforesaid URE and URRE statistics. Let $\overline{\boldsymbol{p}}_i(t)$ and $\overline{\boldsymbol{v}}_i(t)$ denote the relative position and velocity inferred by the ego CAV from the BSMs received from the other vehicles. Then $\boldsymbol{p}_i(t) \sim \mathcal{N}(\overline{\boldsymbol{p}}_i(t), \sigma^2_{\text{URE}} I_{(2)})$ and $\boldsymbol{v}_i(t) \sim \mathcal{N}(\overline{\boldsymbol{v}}_i(t), \sigma^2_{\text{URRE}} I_{(2)})$, where $\sigma_{\text{URE}} = 0.715/2 = 0.3575$ m and $\sigma_{\text{URRE}} = 6\text{E-}3/2 = 3\text{E-}3$ m/s.

TABLE I

ILLUSTRATIVE RESULTS OF MONTE CARLO SAMPLING FOR UNCERTAINTY QUANTIFICATION OF THE THREAT AT $\boldsymbol{p} \in \mathcal{W}$ IN THE 1-CAR SCENARIO.

	$\boldsymbol{p}$ (m)	$\overline{\boldsymbol{p}}_i(t)$ (m)	$\overline{\boldsymbol{v}}_i(t)$ (m/s)	$\mathbb{E}\left[c(\boldsymbol{p},t)\right]$	$Var\left[c(\boldsymbol{p},t)\right]$
1.	$(0,1)$	$(150,0)$	$(0,0)$	2.727E-3	2.227E-6
2.	$(20,1)$	$(150,0)$	$(0,0)$	3.072E-2	2.066E-4
3.	$(40,1)$	$(150,0)$	$(0,0)$	0.2558	1.098E-2
4.	$(0,1)$	$(134.4,0)$	$(-12.5,0)$	3.099	1.298
5.	$(20,1)$	$(134.4,0)$	$(-12.5,0)$	5.033	3.432
6.	$(40,1)$	$(134.4,0)$	$(-12.5,0)$	8.266	9.219
7.	$(0,1)$	$(40.44,0)$	$(-12.53,0)$	30.73	127.5
8.	$(20,1)$	$(40.44,0)$	$(-12.53,0)$	45.77	282.8
9.	$(40,1)$	$(40.44,0)$	$(-12.53,0)$	55.93	422.2

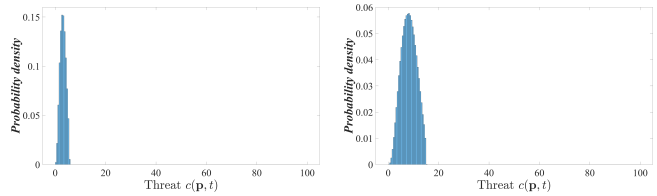

(a) $\boldsymbol{p}, \overline{\boldsymbol{p}}_i(t), \overline{\boldsymbol{v}}_i(t)$ in Row 4. (b) $\boldsymbol{p}, \overline{\boldsymbol{p}}_i(t), \overline{\boldsymbol{v}}_i(t)$ in Row 6.

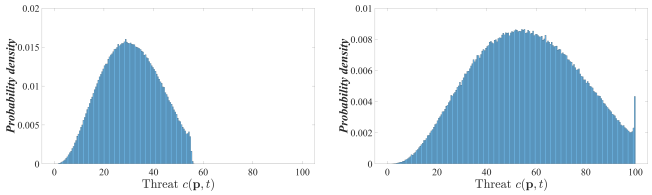

(c) $\boldsymbol{p}, \overline{\boldsymbol{p}}_i(t), \overline{\boldsymbol{v}}_i(t)$ in Row 7. (d) $\boldsymbol{p}, \overline{\boldsymbol{p}}_i(t), \overline{\boldsymbol{v}}_i(t)$ in Row 9.

Fig. 5. Normalized posterior frequency distributions for some of the examples listed in Table I.

TABLE II

ILLUSTRATIVE RESULTS OF MONTE CARLO SAMPLING FOR UNCERTAINTY QUANTIFICATION OF THE THREAT AT $\boldsymbol{p} \in \mathcal{W}$ IN THE 4-CAR SCENARIO.

	$\boldsymbol{p}$ (m)	t (s)	$\mathbb{E}\left[c(\boldsymbol{p},t)\right]$	$Var\left[c(\boldsymbol{p},t)\right]$
1.	$(0,1)$	0	1.629E-1	1.494E-2
2.	$(20,1)$	0	6.313E-2	1.297E-3
3.	$(40,1)$	0	1.664	1.246
4.	$(0,1)$	7.5	7.675	1.833
5.	$(20,1)$	7.5	56.45	56.02
6.	$(40,1)$	7.5	96.20	159.9
7.	$(0,1)$	15	30.87	127.6
8.	$(20,1)$	15	45.79	282.58
9.	$(40,1)$	15	55.92	422.1

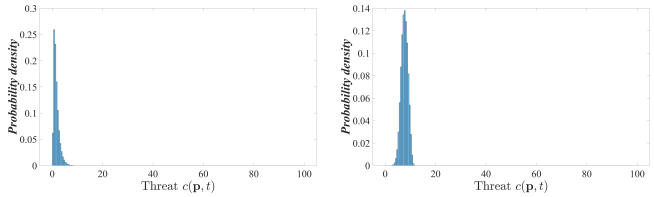

(a) $\boldsymbol{p}, \overline{\boldsymbol{p}}_i(t), \overline{\boldsymbol{v}}_i(t)$ in Row 3. (b) $\boldsymbol{p}, \overline{\boldsymbol{p}}_i(t), \overline{\boldsymbol{v}}_i(t)$ in Row 4.

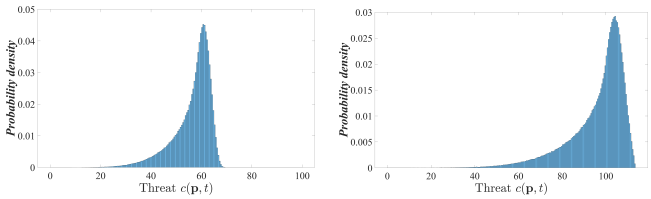

(c) $\boldsymbol{p}, \overline{\boldsymbol{p}}_i(t), \overline{\boldsymbol{v}}_i(t)$ in Row 5. (d) $\boldsymbol{p}, \overline{\boldsymbol{p}}_i(t), \overline{\boldsymbol{v}}_i(t)$ in Row 6.

Fig. 6. Normalized posterior frequency distributions for some of the examples listed in Table II.

For the sake of simplicity, we make several simplifying assumptions including: the position and velocity errors are uncorrelated, the position/velocity errors along orthogonal axes are uncorrelated, and the velocity error standard deviation in each coordinate is the same as the URRE. The numerical values of standard deviations σ_{URE} and σ_{URRE} are calculated with the assumption that GPS user errors are normally distributed. These assumptions will admittedly cause errors in the resultant threat field uncertainty quantification, but they can be removed in further detailed analysis in the future.

We take a large number of samples $\boldsymbol{p}_i, \boldsymbol{v}_i$ from the distributions $\mathcal{N}(\overline{\boldsymbol{p}}_i(t), \sigma^2_{\mathrm{URE}} I_{(2)})$ and $\mathcal{N}(\overline{\boldsymbol{v}}_i(t), \sigma^2_{\mathrm{URRE}} I_{(2)})$. For each sample we evaluate the threat value and calculate posterior statistics (mean and variance) at desired locations $\boldsymbol{p} \in \mathcal{W}$ and time instant t. Table I provides examples of these posterior statistics for the 1-car scenario shown in Fig. 2. Figure 5 illustrates the normalized histogram of the threat values computed for each sample, which is an approximation for the posterior probability density function. Each of these results (i.e., each row in Table I) was obtained by threat evaluations for one million samples of $\boldsymbol{p}_i$ and $\boldsymbol{v}_i$.

The most important observation from the results shown in Table I and Fig. 5 is that the uncertainty in threat (quantified by its variance) can become large even though the uncertainty in position and velocity of surrounding vehicles (quantified, say, by GPS URE and URRE) remains small.

Table II and Fig. 6 illustrate similar results for the 4-car scenario in Figs. 3 and 4.

B. Perturbation Method

An analytical alternative to the Monte Carlo sampling method is the perturbation method, which relies on analyzing the sensitivities of the threat values to the parameters $\boldsymbol{p}_i(t)$ and $\boldsymbol{v}_i(t)$. We denote these parameters by $\boldsymbol{q} = (q_1, \ldots, q_{4N}) = (\ldots, p_{ix}, p_{iy}, v_{ix}, v_{iy}, \ldots)$, the parameter mean and variance by $\overline{\boldsymbol{q}} = (\ldots, \overline{\boldsymbol{p}}_i, \overline{\boldsymbol{v}}_i \ldots)$ and $P = \mathrm{diag}(\ldots, \sigma^2_{\mathrm{URE}}, \sigma^2_{\mathrm{URRE}}, \ldots) \in \mathbb{R}^{4N \times 4N}$, respectively. As in Section III-A, the underlying assumption is that these parameters are normally distributed and mutually independent. The parameter sensitivity gradient is $S = \left.\frac{\partial c}{\partial \boldsymbol{q}}\right|_{\boldsymbol{q}=\overline{\boldsymbol{q}}}$.

It may be shown [14] that the posterior mean and variance can be approximated as

$$\mathbb{E}\left[c(\boldsymbol{p},t)\right] = c(\overline{\boldsymbol{q}},t), \qquad Var\left[c(\boldsymbol{p},t)\right] = SPS^{\mathsf{T}}. \quad (2)$$

This approximation is exact when the parameters are indeed normally distributed and mutually independent, and the func-

TABLE III
ILLUSTRATIVE RESULTS OF PERTURBATION METHOD FOR UNCERTAINTY QUANTIFICATION OF THE THREAT AT $\boldsymbol{p} \in \mathcal{W}$ IN THE 1-CAR SCENARIO.

	$\boldsymbol{p}$ (m)	$\overline{\boldsymbol{p}}_i(t)$ (m)	$\overline{\boldsymbol{v}}_i(t)$ (m/s)	$\mathbb{E}\left[c(\boldsymbol{p},t)\right]$	$Var\left[c(\boldsymbol{p},t)\right]$
1.	$(0,1)$	$(150,0)$	$(0,0)$	1.697E-3	4.430E-7
2.	$(20,1)$	$(150,0)$	$(0,0)$	2.269E-2	8.828E-5
3.	$(40,1)$	$(150,0)$	$(0,0)$	0.2147	7.942E-3
4.	$(0,1)$	$(134.4,0)$	$(-12.5,0)$	3.097	1.642
5.	$(20,1)$	$(134.4,0)$	$(-12.5,0)$	5.033	4.337
6.	$(40,1)$	$(134.4,0)$	$(-12.5,0)$	8.258	11.67
7.	$(0,1)$	$(40.44,0)$	$(-12.53,0)$	30.71	161.4
8.	$(20,1)$	$(40.44,0)$	$(-12.53,0)$	45.74	358.0
9.	$(40,1)$	$(40.44,0)$	$(-12.53,0)$	55.90	534.8

tion c is linear. Per the threat definition in Section II, linearity does not hold for this application. In fact, the threat field definition involves discontinuities due to the sign function. To compute the sensitivity gradient, we approximate the sign function by a sigmoidal function.

Table III shows the posterior mean and variance values computed for the 1-car scenario shown in Fig. 2. Comparing these values to those in Table I, we note accurate results for the posterior mean and order-of-magnitude accuracy for the posterior variance. The variance accuracy may be improved in the future by removing the aforesaid discontinuities.

C. Risk of Planned Trajectories

Consider a short-term trajectory $\boldsymbol{\pi}$ of the ego-CAV in the form of a sequence of spatiotemporal waypoints expressed in the ego-fixed axes system at time $t = 0$, i.e., $\boldsymbol{\pi} = ((\boldsymbol{w}_0, t_0), (\boldsymbol{w}_1, t_1) \ldots, (\boldsymbol{w}_A, t_A))$, where $\boldsymbol{w}_n \in \mathcal{W}$ are spatial locations and t_n are uniformly spaced time instants with fixed $t_n - t_{n-1} = \Delta t$, for $n = 0, 1, \ldots, A$ and for some finite A. The cost of this trajectory is defined as $\mathcal{J}(\boldsymbol{\pi}) := \Delta t \sum_{n=0}^{A} (\lambda + \lambda c(\boldsymbol{w}_n, t))$, where $\lambda \geqslant 0$ is a constant. The expected cost is $\mathbb{E}\left[\mathcal{J}(\boldsymbol{\pi})\right] = \sum_{n=0}^{A} (\lambda + \mathbb{E}\left[c(\boldsymbol{w}_n, t)\right])$. We define the trajectory *risk* $\rho(\boldsymbol{\pi})$ as dependent on the expected cost as well as the threat variances at each waypoint:

$$\rho(\boldsymbol{\pi}) := \mathbb{E}\left[\mathcal{J}(\boldsymbol{\pi})\right] + \Delta t \sqrt{\textstyle\sum_{n=0}^{A} Var\left[c(\boldsymbol{w}_n, t)\right]}.$$

By this definition, a low risk trajectory not only has low expected threat exposure, but also low uncertainty thereof. The expected trajectory cost and risk can be computed using the analysis presented above. For example, in the aforementioned 4-car traffic scenario, consider a trajectory $\boldsymbol{\pi}$ with $\boldsymbol{w}_n = (0, 0)$ for each $n = 0, \ldots, A$, with $\Delta t = 5$E-3 s and $A = 15/(\Delta t) = 3000$. This trajectory corresponds to the ego CAV's steady state of zero acceleration over a 15 s time interval. We choose $\lambda = 0$. Using the Monte Carlo sampling method, the expected cost and risk of this trajectory are:

$$\mathbb{E}\left[\mathcal{J}(\boldsymbol{\pi})\right] = 230.4, \qquad \rho(\boldsymbol{\pi}) = 231.3.$$

Fast analytical method such as the perturbation method can enable the efficient computation of the expected cost and risk for trajectory planning computations.

IV. CONCLUSIONS

In this paper, we proposed a new threat field model for short-term trajectory planning in automated driving. This threat field model provides a framework to fuse V2V data with onboard sensor data, which is mathematically more convenient compared to the probabilistic occupancy grids typically used. We analyzed the effects of uncertainty in the positions and velocities of surrounding vehicles on the threat field. Finally, we quantify risk of planned trajectories based on exposure to the uncertain threat field. Uncertainty quantification is studied using Monte Carlo sampling as well a perturbation-based approach. The main observation of interest is that small uncertainties in positions and velocities of other vehicles can lead to large uncertainties in the threat field and trajectory risk. Future work includes addressing correlations between positions and velocities via uncertainty propagation equations.

REFERENCES

[1] S. Chen, A. M. Wyglinski, S. Pagadarai, R. Vuyyuru, and O. Altintas, "Feasibility analysis of vehicular dynamic spectrum access via queueing theory model," *IEEE Communications Magazine*, vol. 49, no. 11, pp. 156–163, 2011.

[2] Y. Han, D. Chen, and S. Ahn, "Variable speed limit control at fixed freeway bottlenecks using connected vehicles," *Transportation Research Part B*, vol. 98, pp. 113–134, 2017.

[3] H. Park, C. Bhamidipati, and B. Smith, "Development and Evaluation of Enhanced IntelliDrive-Enabled Lane Changing Advisory Algorithm to Address Freeway Merge Conflict," *Transportation Research Record: Journal of the Transportation Research Board*, vol. 2243, pp. 146–157, dec 2011. [Online]. Available: http://dx.doi.org/10.3141/2243-17

[4] J. Rios-Torres, A. Malikopoulos, and P. Pisu, "Online Optimal Control of Connected Vehicles for Efficient Traffic Flow at Merging Roads," in *2015 IEEE 18th International Conference on Intelligent Transportation Systems*, sep 2015, pp. 2432–2437.

[5] D. Chen, S. Ahn, M. Chitturi, and D. A. Noyce, "Towards vehicle automation: Roadway capacity formulation for traffic mixed with regular and automated vehicles," *Transportation Research Part B: Methodological*, vol. 100, pp. 196–221, 2017.

[6] J. Wang, J. Liu, and N. Kato, "Networking and Communications in Autonomous Driving: A Survey," *IEEE Communications Surveys and Tutorials*, vol. 21, no. 2, pp. 1243–1274, apr 2019.

[7] B. Paden, M. Čáp, S. Z. Yong, D. Yershov, and E. Frazzoli, "A survey of motion planning and control techniques for self-driving urban vehicles," *IEEE Trans. Intelligent Vehicles*, vol. 1, no. 1, pp. 33–55, March 2016.

[8] D. González, J. Pérez, V. Milanés, and F. Nashashibi, "A review of motion planning techniques for automated vehicles," *IEEE Trans. Intelligent Transportation Systems*, vol. 17, no. 4, pp. 1135–1145, 2015.

[9] G. Tanzmeister, J. Thomas, D. Wollherr, and M. Buss, "Grid-based mapping and tracking in dynamic environments using a uniform evidential environment representation," in *2014 IEEE International Conference on Robotics and Automation (ICRA)*, May 2014, pp. 6090–6095.

[10] T. Colleens, J. J. Colleens, and D. Ryan, "Occupancy grid mapping: An empirical evaluation," in *2007 Mediterranean Conference on Control Automation*, Jun. 2007, pp. 1–6.

[11] E. Kaufman, T. Lee, Z. Ai, and I. Moskowitz, "Bayesian occupancy grid mapping via an exact inverse sensor model," *2016 American Control Conference (ACC)*, 2016.

[12] L. Eliot, "Tesla on autopilot slams into stalled car on highway, expect more of this," *Forbes*, May 26 2019. [Online]. Available: https://www.forbes.com/sites/lanceeliot/2019/05/26/tesla-on-autopilot-rams-into-stalled-car-on-highway-expect-more-of-this/#448b31094fe5

[13] "GPS: The Global Positioning System: a global public service brought to you by the U.S. government," https://www.gps.gov/, accessed Mar. 03, 2021.

[14] R. C. Smith, *Uncertainty Quantification: Theory, Implementation, and Applications*. Philadelphia, PA, USA: SIAM, 2014.